Influence of magnetization anisotropy on angular magnetoresistance in the antiferromagnetic topological semimetal HoSb

Z.-L. Xia,[1] F. Tang,[1,2] C.-Q. Xu,[3,4] S. Cong,[1] W. Zhao,[5] L. Zhang,[1] Z.-D. Han,[1] B. Qian,[1,*] X.-F. Jiang,[1] X. Ke,[3] and Y. Fang[1,†]

[1]*Jiangsu Laboratory of Advanced Functional Materials, School of Electronic and Information Engineering, Changshu Institute of Technology, Changshu 215500, China*

[2]*Jiangsu Key Laboratory of Thin Films, School of Physical Science and Technology, Soochow University, Suzhou 215006, China*

[3]*Department of Physics and Astronomy, Michigan State University, East Lansing, Michigan 48824, USA*

[4]*School of Physics and Key Laboratory of MEMS of the Ministry of Education, Southeast University, Nanjing 211189, China*

[5]*Department of Materials Science and Engineering, Monash University, Clayton VIC 3800, Australia*

(Received 13 May 2022; revised 26 July 2022; accepted 8 September 2022; published 21 September 2022)

Magnetic rare-earth monopnictides have attracted a great deal of interest, not only because of the nontrivial topological electronic states but also due to the extremely large magnetoresistance. In this paper, we report the angular-dependent magnetization and magnetoresistance of the antiferromagnetic topological semimetal HoSb. At elevated temperatures, the angular magnetoresistance displays minima and maxima around $n\pi/2$ and $(2n+1)\pi/4$ ($n = 0$, 1, 2, and 3), respectively. At low temperatures ($<\sim$6 K), both the magnetoresistance and magnetization showcase strong angular dependence. Different from those of other rare-earth monopnictides, HoSb's angular magnetoresistance exhibits extra minima between $n\pi/2$ and $(2n+1)\pi/4$, and between $(2n+1)\pi/4$ and $(n+1)\pi/2$ ($n = 0$, 1, 2, and 3), around which the magnetic phase transitions from ferromagnetic to HoP-type antiferromagnetic state, and from HoP-type antiferromagnetic to ferromagnetic state occur, suggesting the close interplay between conduction electrons and magnetism. Several possible causes have been carefully discussed for these unexpected phenomena. Our findings reveal the crucial role of magnetization anisotropy on the angular magnetoresistance in magnetic rare-earth monopnictides, and may provide a paradigm for studying the magnetization control of magnetoresistance anisotropy in other magnetic semimetals.

DOI: 10.1103/PhysRevB.106.115137

I. INTRODUCTION

The magnetoresistance (MR) effect has been a long-standing topic in condensed-matter physics and materials science for the complex underlying mechanisms and significant technological impact [1–3]. To date, a large variety of MR phenomena, including the giant MR in magnetic multilayers [4], the colossal MR in mixed-valence manganese/cobalt oxides [5], and the tunneling MR in magnetic tunnel junctions [6], have been extensively reported in the literature. Nevertheless, discovery of the extreme MR (XMR $\sim 10^4\%$–$10^6\%$) in novel materials, such as WTe_2, Cd_3As_2, the *MPn* family ($M =$ Ta and Nb; $Pn =$ P and As), MoP_2, the *RPn* series ($R =$ rare earth; $Pn =$ Sb, and Bi), and so on, still has stimulated a renewed interest in this field over the past few years [7–36]. It has been found that their MR could be derived from either the lifting of topologically protected backscattering by applied magnetic fields ($\mu_0 H$) or Fermi-surface (FS) compensation [7–36]. Significantly, their MR usually shows remarkable anisotropy depending on the angle (φ) between $\mu_0 H$ and current (I), which varies considerably from one system to another. As reported, two material families have attracted enormous attention for their intriguing angular MR. One is the *MPn* family, such as TaAs, TaP, NbAs, and NbP, where positive and negative MR occur for $\mu_0 H \perp I$ and $\mu_0 H // I$, respectively [20,37]. The other one is the *RPn* family that shows twofold and fourfold symmetric MR when I flows along the principal axes, and $\mu_0 H$ rotates in the plane consisting of $\mu_0 H$ and I, and is always perpendicular to I, respectively [38]. Note that special attention has been paid to the latter case, since the *RPn* family crystallizes in a simple-cubic crystal structure and their angular MR can be well reproduced by those classical transport models [39]. More importantly, integrating their high-mobility semimetallic bands with the long-periodic magnetic structures could not only keep the XMR preserved [40], but also provides a promising platform for studying the magnetization- ($M-$) governed MR anisotropy [28,41]. Recently, Xu *et al.* found that at low temperature (T) CeSb's M ($\Gamma_8^{(1)}$ orbital) flops in close proximity to $(2n+1)\pi/4$ with $n = 0$, 1, 2, and 3, and meanwhile the angular MR shows extra minima (except for the ones at $n\pi/2$) [41] that are absent in the nonmagnetic isostructural counterparts [39,42]. Thereafter, similar cases have also been observed in the sister member CeBi [28]. These findings imply that in these Ce monopnictides the conduction electrons have strong interactions with magnetism, and extra minima in the angular MR are possibly

*njqb@cslg.edu.cn
†fangyong@cslg.edu.cn

associated with the M flops [28,41]. Note that their M flops between these easy axes, implying that M anisotropy plays a crucial ingredient in determining the angular MR. It is reported that in those magnetic RPn members (except for Gd monopnictides [43]) the $4f$ orbital moments cannot be quenched by crystal electric fields (CEFs), and consequently their M generally shows significant φ dependence. Thus, M-determined MR anisotropy could be widely expected in these
systems.

Previous studies revealed that most of the RPn series show long-range spin orderings [44]. Among them, the ones with $R =$ Ce, Nd, Dy, and Ho exhibit strong M anisotropy (in agreement with the Ising model) [45], whereas the other ones with $R =$ Tb and Er show less pronounced M anisotropy [26,46]. Recently, it was found that ErBi's and TbSb's angular MR simply follows the trends as observed in La and Lu monopnictides [26,47]. That is, their MR becomes minima at $n\pi/2$ and maxima at $(2n+1)\pi/4$ with $n = 0$, 1, 2, and 3. An analogous case has been uncovered in the orbitally quenched sister member GdBi as well [43]. On the contrary, in Ce monopnictides [48,49], their angular MR at $(2n+1)\pi/4$ ($n =$ 0, 1, 2, and 3) shows minima instead of maxima as observed in the nonmagnetic isostructural analog. It thus could be inferred that additional minima could emerge in the angular MR of those isostructural RPn compounds with strong M anisotropy. HoSb, in which Ho^{3+} is a non–Kramers ion and carries magnetic moments [50], shows a type-II antiferromagnetic (AFM) structure with its ground-state magnetic properties determined by three low-lying levels, including $\Gamma_3^{(2)}$, $\Gamma_4^{(2)}$, and Γ_1 [51]. Due to the presence of strong CEF effects and quadrupolar interactions therein, HoSb's M are confined in the $\langle 100\rangle$ axes [51]. Busch and Vogt further predict that to force its M away from the $\langle 100\rangle$ axes $\mu_0 H \sim 10^2$ T is required [52]. It follows that this compound is strongly anisotropic in M and could serve as an ideal candidate for studying the M-governed MR anisotropy. In this paper, we report HoSb's φ-dependent M and MR at different T and $\mu_0 H$. Above Néel T (T_N), HoSb shows fourfold symmetric angular MR with the minima and maxima in close proximity to $n\pi/2$ and $(2n+1)\pi/4$ ($n = 0$, 1, 2, and 3), respectively. Analogous cases have been frequently observed in these nonmagnetic isostructural counterparts [39,42]. Below T_N, unexpected M minima together with extra MR extrema simultaneously occur between $n\pi/2$ and $(2n+1)\pi/4$, and between $(2n+1)\pi/4$ and $(n+1)\pi/2$ ($n = 0$, 1, 2, and 3). Our work implies that in HoSb its conduction electrons closely couple with magnetism, and supports that M-governed angular MR could be remarkable in magnetic RPn members with strong M anisotropy.

II. EXPERIMENTAL METHODS

HoSb single crystals were grown by the flux method using molten tin as a solvent [32]. The x-ray diffraction pattern (Fig. S1(a) in the Supplemental Material [53]; also see [54]), energy-dispersive x-ray spectra, and element mappings (Figs. S1(b)–S1(e) in the Supplemental Material [53]) were taken with a PANalytical X'Pert PRO diffractometer and a field-emission scanning electron microscope equipped with an energy-dispersive x-ray (EDX) spectrometer, respectively. Magnetic measurements were performed on a Quantum Design MPMS3-SQUID magnetometer. Electrical transports were measured by a standard four-contact method in a Quantum Design physical property measurement system (PPMS-9).

III. RESULTS AND DISCUSSION

Figure 1(a) exhibits the variation of HoSb's M as a function of T under 0.05 T for $\mu_0 H//c$. As delineated, M shows a cusp as emerged in the typical antiferromagnets [32]. Its T_N, as indicated by a sharp peak in the plot of first order derivate of M as a function of T [dM/dT, the inset of Fig. 1(a)], is determined to be ~5.7 K. Figure 1(b) depicts the M isotherm at 2 K for $\mu_0 H//c$. Clearly, a linear increase of M is observed at low $\mu_0 H$ (<1 T), which coincides with the Ising-type AFM ground state. Upon increasing $\mu_0 H$, the devil's staircase M shows two sudden jumps at ~1.5 and 2.4 T, respectively. Above 3.5 T, M starts to saturate and reaches a value of $\sim 9.8\,\mu_B$ (close to $M_s = g_J J = 10\,\mu_B$ for the free Ho^{3+} ion) [55]. Here, g_J is the Landé g factor and J is the total angular momentum. Note that only a M plateau ($\sim\frac{1}{2}M_s$) which is associated with the HoP-type (quadrature) magnetic structures is presented in the $\mu_0 H$ range between 1.6 and 2.4 T [32]. To easily comprehend the low-T magnetic behavior of HoSb, in the inset of Fig. 1(b), we plot the sketch of spin orderings in three different magnetic phases, including the AFM ground state (MnO type), intermediate state (HoP type), and FM state. Figure 1(c) presents the M isotherms at different T_S from 2 to 11 K. It can be seen that the devil's staircase M becomes obscured with the increasing T, and fades away above 6 K ($\sim T_N$). Figure 1(d) plots the T-dependent resistivity (ρ) under 0 and 9 T for HoSb. Here, T is plotted in a logarithmic scale to highlight the $\mu_0 H$ effect on ρ at low T. One can see that the zero-field ρ decreases with T decreasing, which indicates the metallic property in the whole T range. Due to the reduced spin scatterings in the AFM phase, a sudden drop [the inset of Fig. 1(d)] has been observed around T_N in the zero-field ρ. With an application of $\mu_0 H \sim 9$ T, a metal-insulator-like transition and an eye-catching ρ plateau appear at low T. One can find that at 2 K its MR $\sim 1.6 \times 10^4$%, comparable to that reported in Ref. [32], affirming good sample quality.

As mentioned above, strong M anisotropy can be expected in some RPn members [45], and has exactly been observed in CeSb, DySb, and so on [41,56]. For HoSb, as plotted in Fig. S2(a) of the Supplemental Material [53], M at 20 K shows small φ dependence under different $\mu_0 H$s, which implies that its M anisotropy is weak at the PM state. Here, $\mu_0 H$ rotates in the bc plane, and φ is measured from the [001] axis. With decreasing T to 6 K, M shown in Fig. S2(b) of the Supplemental Material [53] exhibits significant φ dependence, and its anisotropy becomes more pronounced under large $\mu_0 H$. This is especially true at 2 K. As plotted in Fig. 2(a), HoSb's M below 2 T show its minima and maxima at $\sim n\pi/2$ and $\sim(2n+1)\pi/4$ ($n = 0$, 1, 2, and 3), respectively, but maxima at $\sim n\pi/2$ and $\sim(2n+1)\pi/4$ ($n = 0$, 1, 2, and 3) with minima in between under $\mu_0 H \sim 2.5$–7 T. To understand this complicated φ dependence of magnetic

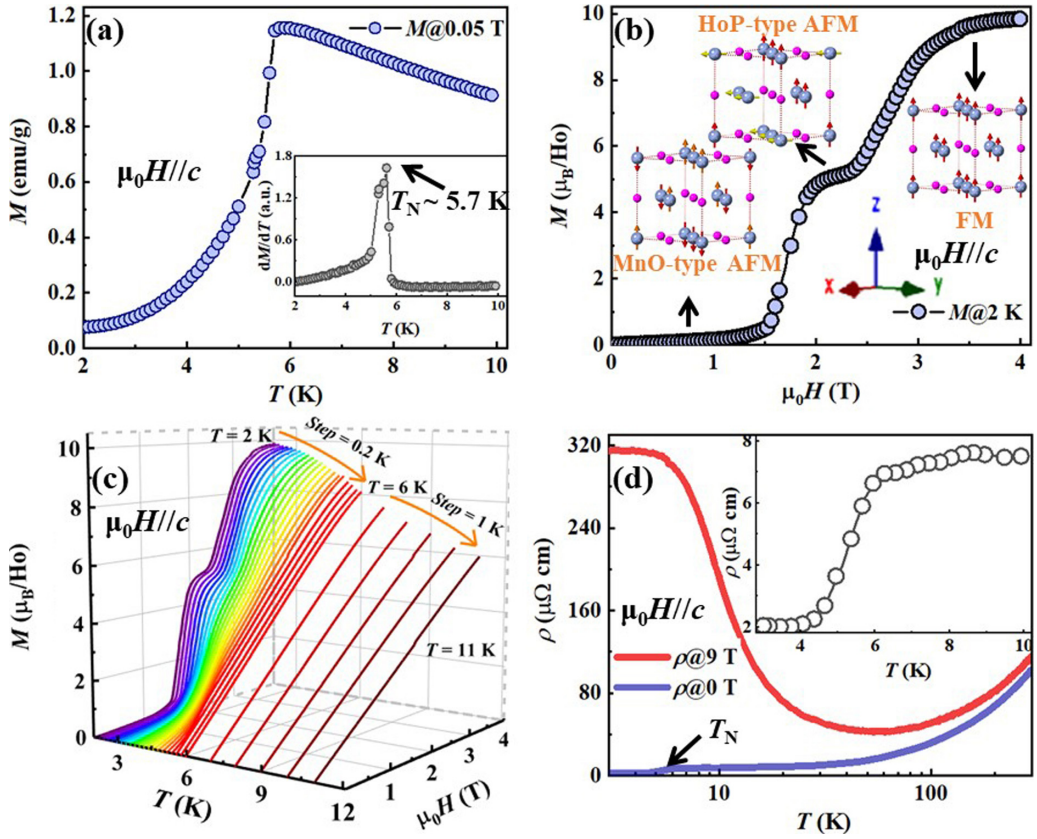

FIG. 1. (a) M as a function of T under 0.05 T for HoSb. The inset shows the T dependence of dM/dT. (b) The M isotherm measured up to 4 T at 2 K. The inset plots the schematic magnetic structures for HoSb's MnO-type AFM, HoP-type AFM, and FM states. (c) M isotherms for $\mu_c H//c$ measured up to 4 T in the T range from 2 to 11 K. (d) ρ vs T at 0 and 9 T for HoSb. The inset shows the low-T ρ under 0 T. Here, I flows along the a axis; $\mu_0 H$ is applied along the c axis.

behaviors, we further measure the isothermal M at 2 K and $\varphi = 45^\circ$ up to 7 T. Here, for reference, the M isotherm for $\mu_0 H//c$ is replotted. One can see that in Fig. 2(b) only a plateau with $M = 6.7\,\mu_B$ ($\sim\sqrt{\frac{1}{2}}M_s$) occurs in the M isotherm for $\varphi = 45^\circ$, and its onset $\mu_0 H$ ($\mu_0 H_c$) decreases from 1.6 T for $\varphi = 0^\circ$ to 1.1 T ($\sim\sqrt{\frac{1}{2}} \times 1.5$) for $\varphi = 45^\circ$. This finding implies that under $\mu_0 H > \sim 1$ T, HoSb enters its HoP-type AFM states around $(2n+1)\pi/4$ ($n = 0$, 1, 2, and 3). Brun *et al.* reported similar M behaviors in Ref. [57], and built the T-$\mu_0 H$ magnetic diagram for the $\mu_0 H//\langle 100\rangle$, $\langle 110\rangle$, and $\langle 111\rangle$ axes, from which the spin configurations under different $\mu_0 H$ can be easily identified. They also clarified that due to strong CEF and quadrupolar interactions the spins should always be pinned along the primary axis, and thus HoSb could be simply treated as a uniaxial antiferromagnet [57]. Further, Busch *et al.* revealed that for M plateaus their $\mu_0 H_c \sim 1/M$ [44]. Provided that this system is in the HoP-type AFM phase, its $M = M_s\sqrt{\frac{1}{2}}|\sin[\varphi + \frac{(2n+1)\pi}{4}]|$ with $n = 0$, 1, 2, and 3 for $0 \leqslant \varphi \leqslant \pi/2$, $\pi/2 \leqslant \varphi \leqslant \pi$, $\pi \leqslant \varphi \leqslant 3\pi/2$, and $3\pi/2 \leqslant \varphi \leqslant 2\pi$, respectively. One can clearly see that with

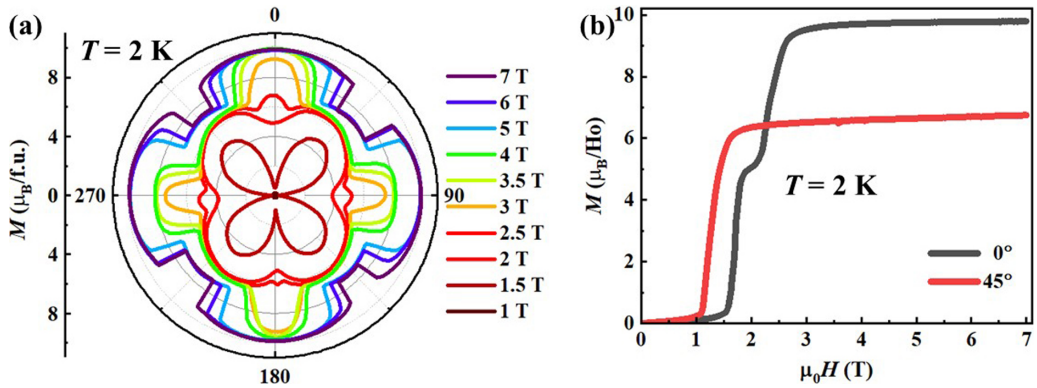

FIG. 2. (a) φ dependence of M under different $\mu_c H$s for HoSb at 2 K. Here, φ is measured from the c axis. (b) M isotherms at 0 and 45° for HoSb.

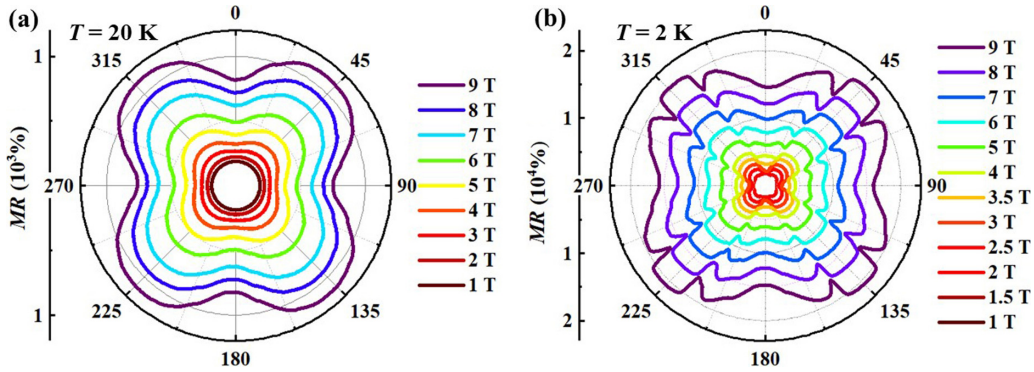

FIG. 3. Angular MR under different $\mu_c H$s at (a) 20 K, and (b) 2 K. Here, I flows along the a axis, $\mu_0 H$ rotates in the bc plane, and φ is measured from the c axis.

φ increasing from $n\pi/2$ $[(2n+1)\pi/4]$ to $(2n+1)\pi/4$ $[(n+1)\pi/2]$ ($n = 0$, 1, 2, and 3), M monotonically increases (decreases), whereas $\mu_0 H_c$ uniformly decreases (increases).

Next, we attempt to figure out the variation of M as a function of φ at various $\mu_0 H$s and 2 K. Under a rotating $\mu_0 H \sim 1$–2 T, HoSb shows the MnO-type AFM state and HoP-type AFM state around $n\pi/2$ and $(2n+1)\pi/4$ ($i = 0$, 1, 2, and 3), respectively, or the HoP-type AFM state in the whole φ range. In this case, its M minima are expected to be around $n\pi/2$ and M maxima should be presented in proximity to $(2n+1)\pi/4$ ($i = 0$, 1, 2, and 3). Under a rotating $\mu_0 H >$ 2.5 T, HoSb exhibits FM and HoP-type AFM states around $n\pi/2$ and $(2n+1)\pi/4$ ($i = 0$, 1, 2, and 3), respectively. In this situation, M maxima are supposed to be around $n\pi/2$ and $(2n+1)\pi/4$, and M minima should emerge between $n\pi/2$ $[(2n+1)\pi/4]$ and $(2n+1)\pi/4$ $[(n+1)\pi/2]$ ($i = 0$, 1, 2, and 3). Obviously, these cases appear to agree with the angular M in Fig. 2(a).

As the *RPn* family crystallizes in a rocksalt cubic crystal lattice with the space group $Fm\bar{3}m$, their band structures share similarities along the k_x, k_y, and k_z directions of the Brillouin zone [10,21,23,26,28,38,41,47]. One could draw attention to the presence of almost equal and sizable electron and hole pockets in their FS. More importantly, it has been found that several intriguing phenomena, such as the pseudo-two-dimensional transport [42], strong $\mu_0 H$-induced valley polarization [58], etc., are always related to the highly anisotropic electron FS sheets. It is precisely because of these properties that MR in these nonmagnetic *RPn* series generally shows quadratic $(\mu_0 H)^2$ dependences [20,36], and significant φ dependences governed by their FS anisotropy [39,42]. Similar cases have been observed in those isostructural analogs with weak M anisotropy, such as TbSb, ErBi, and GdBi [26,41,47], whereas Ce monopnictides [28,41], where their M exhibits remarkable anisotropy and has significant influence on conduction electrons, present M-tunable angular MR. Thus, HoSb, an Ising-type AFM system with highly anisotropic M, is expected to show similar MR behaviors.

To verify these hypotheses, we perform angular MR measurements under different $\mu_0 H$s above and below T_N. Here, I flows along the a axis, $\mu_0 H$ rotates in the bc plane (i.e., $\mu_0 H$ is always perpendicular to I), and φ is measured from the c axis. Figure 3(a) shows MR as a function of φ under various $\mu_0 H$s for HoSb at 20 K. It is clear that all the angular MR always show a fourfold symmetry, and minima and maxima at $n\pi/2$ and $(2n+1)\pi/4$ ($n = 0$, 1, 2, and 3), respectively, which is in good agreement with the cubic crystal structure [59]. In Fig. S3(a) of the Supplemental Material [53], one can also see that the angular MR at 15 K share similarity in φ dependences under various $\mu_0 H$s and resemble those at 20 K, implying that FS anisotropy plays a major role. Figure 3(b) exhibits HoSb's MR as a function of φ under different $\mu_0 H$s at 2 K. It is obvious that the angular MR has been significantly altered but its fourfold symmetry remains unchanged, which highlights the effect of FS anisotropy or cubic crystal symmetry on the φ-dependent transport. Below 1.5 T, the angular MR (Fig. S3(b) in the Supplemental Material [53]) shows its minima and maxima around $n\pi/2$ and $(2n+1)\pi/4$ ($n = 0$, 1, 2, and 3), respectively. Above 2 T, extra MR extrema appear between $n\pi/2$ and $(2n+1)\pi/4$, and between $(2n+1)\pi/4$ and $(n+1)\pi/2$ ($n = 0$, 1, 2, and 3), which are clearly visible above 3.5 T (Fig. S3(b) in the Supplemental Material [53]). Note that we have measured the angular MR at 4 and 6 K up to 9 T (Figs. S3(c) and S3(d) in the Supplemental Material [53]), and observed similar phenomena below T_N (~6 K). More importantly, one can see that the corresponding φs for HoSb's MR minima, i.e., the ones in proximity to $n\pi/2$ under $\mu_0 H < 1.5$ T, and the ones between $n\pi/2$ $[(2n+1)\pi/4]$ and $(2n+1)\pi/4$ $[(n+1)\pi/2]$ ($n = 0$, 1, 2, and 3) under $\mu_0 H >$ 2 T in Fig. 3(b), almost take the values around which the angular M in Fig. 2(a) exhibits minima as well. These findings are indicative of a certain correlation between the angular M and MR of HoSb.

As presented in Ref. [41], CeSb's MR show additional minima at $(2n+1)\pi/4$ ($n = 0$, 1, 2, and 3). This is because in this compound the planar $\Gamma_8^{(1)}$ orbital governed M always aligns along these primary axes, and once $\mu_0 H$ crosses $(2n+1)\pi/4$ ($n = 0$, 1, 2, and 3) M flops and meanwhile the generated magnetic multidomains enhance electron scatterings. For HoSb, its M lies on the a, b, and c axes at the ground state [57]. Note that its M depends on the strong CEF effect and quadrupolar interactions thereof [51], and could hardly be diverted from those easy M axes [52]. Namely, in HoSb M flop could not be readily accessible. This feature is supported by MR isotherm measurements at different φs and 2 K. As shown in Fig. S4 of the Supplemental Material [53], MR isotherms change their shapes from one to another

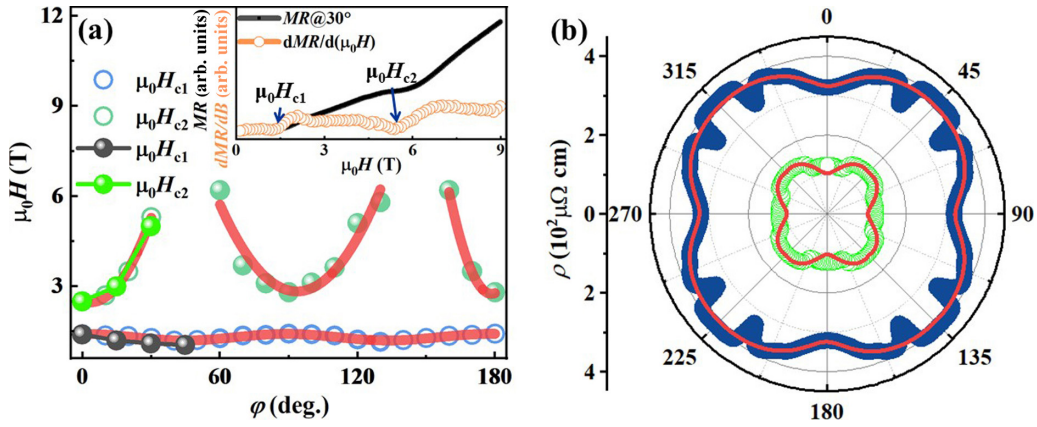

FIG. 4. (a) $\mu_0 H_{c1}$ and $\mu_0 H_{c2}$ as a function of φ at 2 K. Here, $\mu_0 H$s are extracted from both the isothermal MR and M. Open circles denote the $\mu_0 H$s deduced from MR isotherms. Solid spheres are $\mu_0 H$s obtained from the M isotherms in Fig. S5 of the Supplemental Material [53]. The inset exhibits the $d\mathrm{MR}/d(\mu_0 H)$ as a function of T at 2 K and 30°, in which the two arrows designate $\mu_0 H_{c1}$ and $\mu_0 H_{c1}$, respectively. For reference, the MR isotherm at 2 K and 30° is replotted. (b) Comparison of the experimental (symbols) and calculated (red solid lines) angular MR under 9 and 4 T at 2 K.

when φ is rotated from the c axis to the $-c$ axis. Here, I flows along the a axis, and $\mu_0 H$ rotates in the bc plane. If HoSb's M flops as observed in Ce monopnictides, these MR isotherms are expected to show similar $\mu_0 H$ dependence at an interval of 90°, and at those complementary and supplementary φs, due to the cubic crystal structure, while the MR isotherm at 30° slightly deviates from that at 60° (120° and 150°), but is likely to follow the trend as observed in the one at 130°. One also can see that these MR isotherms at 20° and 60° share similarities with those at 170° and 160°, respectively. All these findings could be associated with the lattice distortions at low T, magnetostriction, small sample misalignments, etc. [28,41,47,59]. Nevertheless, this finding cannot be a smoking gun for the occurrence of M flop in HoSb. As reported in Refs. [28,41], M flop in Ce monopnictides is confirmed by the cyclic variation of $\mu_0 H_{\mathrm{FM}}$ (the critical $\mu_0 H$ for the FM state in M isotherms) with a period of $\sim\pi/2$, since their M is always pinned in the primary axes and the magnetic phase transitions are dominated by $\mu_0 H$ components along these orientations [28,41]. It is apparent that for $0° \leqslant \varphi \leqslant 30°$, $60° \leqslant \varphi \leqslant 130°$, and $160° \leqslant \varphi \leqslant 180°$ in Fig. S4 of the Supplemental Material [53], two clear kinks corresponding to the $\mu_0 H-$induced magnetic phase transitions from MnO-type to HoP-type AFM state and from HoP-type AFM to FM state, respectively, appear in HoSb's MR isotherms. In the inset of Fig. 4(a), we plot the first derivative of MR with respect to $\mu_0 H$ ($d\mathrm{MR}/d\mu_0 H$) at $\varphi = 30°$. For reference, its MR isotherm counterpart is also plotted. Here, the critical $\mu_0 H$s, including $\mu_0 H_{c1}$ and $\mu_0 H_{c2}$, indexed to those two kinks are highlighted by blue solid arrows. Figure 4(a) shows the variation of these two $\mu_0 H_c$s (open circles) as a function of φ, where the red solid lines are guides to the eyes. As seen, both $\mu_0 H_{c1}$ and $\mu_0 H_{c2}$ have significant φ dependence. Analogous cases have been observed in Ce monopnictides where $\mu_0 H_{\mathrm{FM}}$ follows an inverse cosine relationship [28,41]. For HoSb, $\mu_0 H_{c2}$ increases (decreases) once the field is tilted from (to) $n\pi/2$, and is absent around $(2n+1)\pi/4$, while $\mu_0 H_{c1}$ decreases from $\varphi = n\pi/2$ to $(2n+1)\pi/4$, and then again increases to $(n+1)\pi/2$ ($n = 0$, 1, 2, and 3), so that the maxima and minima repeat every $\pi/2$. This finding agrees with the scenario that even under 9 T HoSb is not always in its FM phase, especially for $\varphi \sim (2n+1)\pi/4$ ($n = 0$, 1, 2, and 3). Namely, its M fails to flop in HoSb under the rotating $\mu_0 H \sim 9$ T. Note that in Fig. 2(b) a similar conclusion is reached in HoSb's angular M. Therefore, it is normal to see the absence of MR minima at φs close to $(2n+1)\pi/4$ ($n = 0$, 1, 2, and 3). In Figs. S5(a)–S5(d) of the Supplemental Material [53], we plot the M isotherms at 2 K and various φs, including 0°, 15°, 30°, and 45°. As seen, the isothermal M presents two jumps for $\varphi = 0°$, 15°, and 30°, but only one jump for $\varphi = 45°$. $\mu_0 H_{c1}$ and $\mu_0 H_{c2}$ are marked by brown arrows in the inset of Fig. S5(a) in the Supplemental Material [53]. Clearly, $\mu_0 H_{c1}$ and $\mu_0 H_{c2}$ [solid spheres in Fig. 4(a)] decrease and increase, respectively, with φ increasing from 0° to 45°. This finding suggests that $\mu_0 H_c$s extracted from both the M and MR isotherms show similar φ dependences.

Next, we attempt to understand HoSb's MR extrema in Fig. 3(b) between $n\pi/2$ and $(2n+1)\pi/4$, and between $(2n+1)\pi/4$ and $(n+1)\pi/2$ with $n = 0$, 1, 2, and 3. As outlined, the bulk band structure calculations reveal that in the RPn family their FS consists mainly of three orthogonal and anisotropic electron pockets (α_1, α_2, and α_3) centered around the X points, and two hole pockets (β harbors a nearly spherical FS, and γ has a FS stretched along the ⟨100⟩ axes) located at the Γ point [10,21,23,60,61]. Note that these electron pockets play a key role in φ-dependent physical properties, especially the anisotropic transport. Previously, Han *et al.* have separated respective contributions of electron and hole pockets from the total angular MR in LaSb, and confirmed the predominance of the electron pockets' contribution to the $\mu_0 H$- or φ-dependent MR [39]. Since RPn shares similarity in their electronic band structures, the same method could be adopted to study HoSb's angular MR. According to Ref. [39], the longitudinal $\rho = \rho_{33} = 1/\sigma_{33}^T$, and $\sigma_{33}^T = \sum_k \sigma_{33}^k$ ($k = \alpha_1$, α_2, α_3, β, and γ), where $\sigma_{33}^{\alpha_1} = \sigma_{33}^{10}/[1+\mu_\perp^2/, H^2(\cos^2\varphi + \sin^2\varphi/\lambda_\mu^2)]$, $\sigma_{33}^{\alpha_2} = \sigma_{33}^{20}/[1+\mu_\perp^2/, H^2(\cos^2\varphi/\lambda_\mu^2 + \sin^2\varphi)]$, $\sigma_{33}^{\alpha_3} = \sigma_{33}^{30}/[1+\mu_\perp^2/, H^2/\lambda_\mu^2]$, and $\sigma_{33}^h = \sigma_{33}^{h0}/(1+\mu_H^2/, H^2/\lambda_\mu^2)$ with $\sigma_{33}^{10} = n_{\alpha 1} e \mu_\perp$,

$\sigma_{33}^{20} = n_{\alpha 2} e \mu_{\perp}$, and $\sigma_{33}^{30} = n_{\alpha 3} e \mu_{//}$ being the respective zero-field σ for α_1, α_2, and α_3, and σ_{33}^{h0} denoting the zero-field σ for combined hole bands (β and γ), $\mu_{\perp}$, $\mu_{//}$, and μ_{H} representing the respective mobility along the long and short axes of electron pockets, and hole pockets, $\lambda_{\mathrm{u}}^2 = \mu_{\perp}/\mu_{//}$. Note that above a rotating $\mu_0 H \sim 3.5\,\mathrm{T}$, HoSb's angular MR exhibits extra extrema at φs where the magnetic phase transition from FM to HoP-type AFM state and from HoP-type AFM to FM state occur. Thus, to reproduce the angular MR under $\mu_0 H > 3.5\,\mathrm{T}$, we cannot simply follow the procedures as performed in Ref. [39]. For HoSb, the φ-dependent $B_{\varphi} = \mu_0 H + M$ should have two different forms (Fig. S6 in the Supplemental Material [53]): $M = M_{\mathrm{s}} \cos(\varphi – \mathrm{n}\pi/2)$ at the FM state around the primary axes and $M_{\mathrm{s}}\sqrt{\frac{1}{2}}|\sin[\varphi + \frac{(2\mathrm{n}+1)\pi}{4}]|$ at the HoP-type AFM state in the proximity of $(2n+1)\pi/4$ with $n = 0$, 1, 2, and 3 for $0 \leqslant \varphi \leqslant \pi/2$, $\pi/2 \leqslant \varphi \leqslant \pi$, $\pi \leqslant \varphi \leqslant 3\pi/2$, and $3\pi/2 \leqslant \varphi \leqslant 2\pi$, respectively. In Fig. 4(b), we plot the calculated angular MR (red solid lines) under 4 and 9 T, in which the contributions from bulk FS and magnetic phase transitions have been taken into account. Here, for simplification, only two elliptical electron pockets and one isotropic hole pocket are considered [28,39,41]. As seen, the experimental angular MR can be well reproduced, from which at 9 T the derived $\lambda_{\mathrm{u}} = 3.8$, $\sigma_{33}^{10} = \sigma_{33}^{20} = 7.25 \times 10^5\,\mathrm{S\,cm^{-1}}$, $\sigma_{33}^{\mathrm{h0}} = 4.1 \times 10^5\,\mathrm{S\,cm^{-1}}$, $\mu_{\perp} = 9.65\,\mathrm{m^2\,V^{-1}\,S^{-1}}$, $\mu_{//} = \mu_{\perp}/\lambda_{\mathrm{u}}^2 = 0.67\,\mathrm{m^2\,V^{-1}\,S^{-1}}$, and $\mu_{\mathrm{H}} = 2.86\,\mathrm{m^2\,V^{-1}\,S^{-1}}$ for the FM phase, and $\sigma_{33}^{10} = \sigma_{33}^{20} = 8.42 \times 10^5\,\mathrm{S\,cm^{-1}}$, $\sigma_{33}^{\mathrm{h0}} = 5.35 \times 10^5\,\mathrm{S\,cm^{-1}}$, $\mu_{\perp} = 8.36\,\mathrm{m^2\,V^{-1}\,S^{-1}}$, $\mu_{//} = \mu_{\perp}/\lambda_{\mathrm{u}}^2 = 0.58\,\mathrm{m^2\,V^{-1}\,S^{-1}}$, and $\mu_{\mathrm{H}} = 3.36\,\mathrm{m^2\,V^{-1}\,S^{-1}}$ for the HoP-type AFM phase. It is clearly visible that the obtained parameters are very close to ones extracted from LaSb [39], suggesting that our fitting results are acceptable. Note that significant divergences between the experimental and calculated angular MR occur at φs between $n\pi/2$ and $(2n+1)\pi/4$, and between $(2n+1)\pi/4$ and $(n+1)\pi/2$ ($n = 0$, 1, 2, and 3), around which the magnetic phase transitions occur, implying that in the title compound its M anisotropy appears not to be directly responsible for these pronounced MR extrema. Similar cases have been observed in CeSb [41]. Xu *et al.* reproduced its angular MR by employing the isotropic and anisotropic B, respectively, and found that the two calculated curves share almost the same shapes. The magnetic multidomain states induced by M flops have been proposed to be a possible cause for these extra minima in CeSb's angular MR [41]. This scenario could be applicable for the minima in HoSb's angular MR between $n\pi/2$ and $(2n+1)\pi/4$, and between $(2n+1)\pi/4$ and $(n+1)\pi/2$ ($n = 0$, 1, 2, and 3). When HoSb experiences the magnetic phase transition from FM to HoP-type AFM state, and from HoP-type AFM to FM state, the magnetic multidomain states could be produced, which enhances the scatterings at domain walls and reduces the carrier mobility, yielding a significantly suppressed MR (MR $\sim \mu_{\mathrm{ave}}^2$; μ_{ave} is the average carrier mobility [10,23,26,38]). Note that in rare earth based intermetallic compounds, such as $SmMn_2Ge_2$ [62], $EuFe_2As_2$ [63], $CeFe_2$ [64], and so on, the superzone boundary effect sometimes gives rise to MR anomalies. The superzone boundary effect is characterized by the vanishing of some parts of FS near the AFM zone boundaries owing to the superzone gap formation [65]. If so, the effective number of conduction electrons decreases and larger ρ emerges at the AFM state [65]. As reported, HoSb and DySb share similarity in their magnetic structures [66], and in the latter one its de Haas–van Alphen oscillations suggest that the FSs at HoP-type AFM and FM states are slightly different [35]. Stimulated by these findings, we perform the band-structure calculations on HoSb. Here, we expand its primitive cell for convenience in comparing the electronic properties at these two states. Figure S7(a) in the Supplemental Material [53] shows the band structures at the FM state, where several bands pass through the Fermi level. Compared to those of the nonmagnetic state [59], all the bands are split possibly due to field-induced broken time-reversal symmetry. The lower panel of Fig. S7(a) in the Supplemental Material [53] plots the corresponding FS sheets of these bands. Their colors are depicted in a one to one relationship. As seen, two sets of electron pockets (α and α') center at the X point and extend along the Γ-X line, and four hole pockets (β, β', γ, and γ') locate at the Γ point. Figure S7(b) in the Supplemental Material [53] displays the band structures in the HoP-type AFM phase. As shown, the band structures at this magnetic state are similar to those at the FM state. It also can be found in the lower panel of Fig. S7(b) in the Supplemental Material [53] that the FS sheets share similarities with those at FM states as well. Thus, our theoretical calculations suggest that the bulk band structures have not been significantly altered when HoSb experiences the magnetic phase transition from FM to HoP-type AFM states and vice versa. Besides, according to the expectation from superzone boundary effects, HoSb should show larger MR in the HoP-type AFM phase. In sharp contrast, its angular MR shows minima when the magnetic phase transitions from FM to the HoP-type AFM state, and from HoP-type AFM to the FM state occur. These findings suggest that the superzone boundary effect cannot be accountable for these unexpected extrema in HoSb's angular MR. Therefore, the magnetic multidomain states could temporarily serve as a possible cause for these phenomena. Of course, this conjecture is yet to be elucidated.

IV. CONCLUSION

In summary, we study the angular M and MR at different $\mu_0 H$s and Ts in the AFM topological semimetal HoSb. Above T_{N}, one can find that its M shows a featureless φ dependence, and its angular MR shares similarity with those as observed in La, Y, Gd, and Lu monopnictides, suggesting that FS anisotropy and crystalline symmetry play a major role. Below T_{N}, due to the presence of strong CEF effect and strong quadrupolar interactions, extra extrema resulting from magnetic phase transitions occur in HoSb's angular M between $n\pi/2$ and $(2n+1)\pi/4$, and between $(2n+1)\pi/4$ and $(n+1)\pi/2$ ($n = 0$, 1, 2, and 3), which is different from those as observed in Ce monopnictides. Meanwhile, its angular MR shows unexpected extrema, i.e., except for the MR minima and maxima at $n\pi/2$ and $(2n+1)\pi/4$ ($n = 0$, 1, 2, and 3), respectively. These findings indicate that the conduction electrons strongly couple with its magnetism in HoSb.

Compared to those as observed in other rare-earth monopnictides, HoSb's angular MR appear to be unique, which could be a result of the competition of multiple factors, such as the anisotropic FS topology, magnetic phase transitions, and so on. Our study highlights the key role of M anisotropy in determining HoSb's angular MR, and could stimulate further work on angular MR and M in other RPn, such as Nd and Dy monopnictides.

ACKNOWLEDGMENTS

This work is supported by the National Natural Science Foundation of China (Grant No. 12174039), Key University Science Research Project of Jiangsu Province (Grant No. 19KJA530003), and Open Fund of Fujian Provincial Key Laboratory of Quantum Manipulation and New Energy Materials (Grant No. QMNEM1903).

Z.-L.X. and F.T. contributed equally to this work.

[1] L. Zhang, J. Zhou, H. Li, L. Shen, and Y. Feng, Appl. Phys. Rev. **8**, 021308 (2021).
[2] M. Tanaka, Jpn. J. Appl. Phys. **60**, 010101 (2021).
[3] R. Niu and W. K. Zhu, J. Phys.: Condens. Matter **34**, 113001 (2022).
[4] J. Torrejon, A. Solignac, C. Chopin, J. Moulin, A. Doll, E. Paul, C. Fermon, and M. Pannetier-Lecoeur, Phys. Rev. Appl. **13**, 034031 (2020).
[5] M. Yen, Y.-H. Lai, C.-Y. Kuo, C.-T. Chen, C.-F. Chang, and Y.-H. Chu, Adv. Funct. Mater. **30**, 2004597 (2020).
[6] S. Yasui, S. Honda, J. Okabayashi, T. Yanase, T. Shimada, and T. Nagahama, Phys. Rev. Appl. **15**, 034042 (2021).
[7] M. N. Ali, J. Xiong, S. Flynn, J. Tao, Q. D. Gibson, L. M. Schoop, T. Liang, N. Haldolaarachchige, M. Hirschberger, N. P. Ong, and R. J. Cava, Nature (London) **514**, 205 (2014).
[8] T. Liang, Q. Gibson, M. N. Ali, M. Liu, R. J. Cava, and N. P. Ong, Nat. Mater. **14**, 280 (2015).
[9] C. Shekhar, A. K. Nayak, Y. Sun, M. Schmidt, M. Nicklas, I. Leermakers, U. Zeitler, Y. Skourski, J. Wosnitza, Z. Liu, Y. Chen, W. Schnelle, H. Borrmann, Y. Grin, C. Felser, and B. Yan, Nat. Phys. **11**, 645 (2015).
[10] F. F. Tafti, Q. D. Gibson, S. K. Kushwaha, N. Haldolaarachchige, and R. J. Cava, Nat. Phys. **12**, 272 (2016).
[11] R. Singha, A. K. Pariari, B. Satpati, and P. Mandal, Proc. Natl. Acad. Sci. USA **114**, 2468 (2017).
[12] J. Y. Liu, J. Hu, Q. Zhang, D. Graf, H. B. Cao, S. M. A. Radmanesh, D. J. Adams, Y. L. Zhu, G. F. Cheng, X. Liu, W. A. Phelan, J. Wei, M. Jaime, F. Balakirev, D. A. Tennant, J. F. DiTusa, I. Chiorescu, L. Spinu, and Z. Q. Mao, Nat. Mater. **16**, 905 (2017).
[13] W. Gao, N. Hao, F.-W. Zheng, W. Ning, M. Wu, X. Zhu, G. Zheng, J. Zhang, J. Lu, H. Zhang, C. Xi, J. Yang, H. Du, P. Zhang, Y. Zhang, and M. Tian, Phys. Rev. Lett. **118**, 256601 (2017).
[14] N. Kumar, Y. Sun, N. Xu, K. Manna, M. Yao, V. Süss, I. Leermakers, O. Young, T. Förster, M. Schmidt, H. Borrmann, B. Yan, U. Zeitler, M. Shi, C. Felser, and C. Shekhar, Nat. Commun. **8**, 1642 (2017).
[15] Y.-Y. Lv, X. Li, J. Zhang, B. Pang, S.-S. Chen, L. Cao, B.-B. Zhang, D. Lin, Y. B. Chen, S.-H. Yao, J. Zhou, S.-T. Zhang, M.-H. Lu, M. Tian, and Y.-F. Chen, Phys. Rev. B **97**, 245151 (2018).
[16] L. Zhao, J. He, D. Chen, S. Zhang, Z. Ren, and G. Chen, Phys. Rev. B **99**, 205116 (2019).
[17] W. Xie, Y. Wu, F. Du, A. Wang, H. Su, Y. Chen, Z. Y. Nie, S.-K. Mo, M. Smidman, C. Cao, Y. Liu, T. Takabatake, and H. Q. Yuan, Phys. Rev. B **101**, 085132 (2020).
[18] J. Bannies, E. Razzoli, M. Michiardi, H.-H. Kung, I. S. Elfimov, M. Yao, A. Fedorov, J. Fink, C. Jozwiak, A. Bostwick, E. Rotenberg, A. Damascelli, and C. Felser, Phys. Rev. B **103**, 155144 (2021).
[19] L. P. He, X. C. Hong, J. K. Dong, J. Pan, Z. Zhang, J. Zhang, and S. Y. Li, Phys. Rev. Lett. **113**, 246402 (2014).
[20] F. Arnold, M. Naumann, S.-C. Wu, Y. Sun, M. Schmidt, H. Borrmann, C. Felser, B. Yan, and E. Hassinger, Phys. Rev. Lett. **117**, 146401 (2016).
[21] J. J. Song, F. Tang, W. Zhou, Y. Fang, H. L. Yu, Z. D. Han, B. Qian, X. F. Jiang, D. H. Wang, and Y. W. Du, J. Mater. Chem. C **6**, 3026 (2018).
[22] O. Pavlosiuk, P. Swatek, D. Kaczorowski, and P. Wiśniewski, Phys. Rev. B **97**, 235132 (2018).
[23] Z. M. Wu, Y. R. Ruan, F. Tang, L. Zhang, Y. Fang, J.-M. Zhang, Z. D. Han, R. J. Tang, B. Qian, and X. F. Jiang, New J. Phys. **21**, 093063 (2019).
[24] S. Sun, Q. Wang, P.-J. Guo, K. Liu, and H. Lei, New J. Phys. **18**, 082002 (2016).
[25] F. Wu, C. Y. Guo, M. Smidman, J. L. Zhang, and H. Q. Yuan, Phys. Rev. B **96**, 125122 (2017).
[26] L.-Y. Fan, F. Tang, W. Z. Meng, W. Zhao, L. Zhang, Z. D. Han, B. Qian, X.-F. Jiang, X. M. Zhang, and Y. Fang, Phys. Rev. B **102**, 104417 (2020).
[27] X. He, C. Zhao, H. Yang, J. Wang, K. Cheng, S. Jiang, L. Zhao, Y. Li, C. Cao, Z. Zhu, S. Wang, Y. Luo, and L. Li, Phys. Rev. B **101**, 075106 (2020).
[28] Y.-Y. Lyu, F. Han, Z.-L. Xiao, J. Xu, Y.-L. Wang, H.-B. Wang, J.-K. Bao, D. Y. Chung, M. Li, I. Martin, U. Welp, M. G. Kanatzidis, and W.-K. Kwok, Phys. Rev. B **100**, 180407(R) (2019).
[29] Y. Fang, F. Tang, Y. R. Ruan, J. M. Zhang, H. Zhang, H. Gu, W. Y. Zhao, Z. D. Han, W. Tian, B. Qian, X. F. Jiang, X. M. Zhang, and X. Ke, Phys. Rev. B **101**, 094424 (2020).
[30] Y. J. Hu, E. I. Paredes Aulestia, K. F. Tse, C. N. Kuo, J. Y. Zhu, C. S. Lue, K. T. Lai, and S. K. Goh, Phys. Rev. B **98**, 035133 (2018).
[31] Y. Zhou, X. Zhu, S. Huang, X. Chen, Y. Zhou, C. An, B. Zhang, Y. Yuan, Z. Xia, C. Gu, and Z. Yang, Phys. Rev. B **96**, 205122 (2017).
[32] Y.-Y. Wang, L.-L. Sun, S. Xu, Y. Su, and T.-L. Xia, Phys. Rev. B **98**, 045137 (2018).
[33] Y.-Y. Wang, H. Zhang, X.-Q. Lu, L.-L. Sun, S. Xu, Z.-Y. Lu, K. Liu, S. Zhou, and T.-L. Xia, Phys. Rev. B **97**, 085137 (2018).
[34] H.-Y. Yang, J. Gaudet, A. A. Aczel, D. E. Graf, P. Blaha, B. D. Gaulin, and F. Tafti, Phys. Rev. B **98**, 045136 (2018).
[35] D. D. Liang, Y. J. Wang, C. Y. Xi, W. L. Zhen, J. Yang, L. Pi, W. K. Zhu, and C. J. Zhang, APL Mater. **6**, 086105 (2018).

[36] L. Ye, T. Suzuki, C. R. Wicker, and J. G. Checkelsky, Phys. Rev. B **97**, 081108(R) (2018).
[37] X. Huang, L. Zhao, Y. Long, P. Wang, D. Chen, Z. Yang, H. Liang, M. Xue, H. Weng, Z. Fang, X. Dai, and G. Chen, Phys. Rev. X **5**, 031023 (2015).
[38] H. Gu, F. Tang, Y.-R. Ruan, J.-M. Zhang, R.-J. Tang, W. Zhao, R. Zhao, L. Zhang, Z.-D. Han, B. Qian, X.-F. Jiang, and Y. Fang, Phys. Rev. Mater. **4**, 124204 (2020).
[39] F. Han, J. Xu, A. S. Botana, Z. L. Xiao, Y. L. Wang, W. G. Yang, D. Y. Chung, M. G. Kanatzidis, M. R. Norman, G. W. Crabtree, and W. K. Kwok, Phys. Rev. B **96**, 125112 (2017).
[40] S. Khalid, A. Sharan, and A. Janotti, Phys. Rev. B **101**, 125105 (2020).
[41] J. Xu, F. Wu, J.-K. Bao, F. Han, Z.-L. Xiao, I. Martin, Y.-Y. Lyu, Y.-L. Wang, D. Y. Chung, M. Li, W. Zhang, J. E. Pearson, J. S. Jiang, M. G. Kanatzidis, and W.-K. Kwok, Nat. Commun. **10**, 2875 (2019).
[42] N. Kumar, C. Shekhar, S.-C. Wu, I. Leermakers, O. Young, U. Zeitler, B. Yan, and C. Felser, Phys. Rev. B **93**, 241106(R) (2016).
[43] D. B. Ghosh, M. De, and S. K. De, Phys. Rev. B **72**, 045140 (2005).
[44] G. Busch, O. Marinček, A. Menth, and O. Vogt, Phys. Lett. **14**, 262 (1965).
[45] G. Busch and O. Vogt, J. Appl. Phys. **39**, 1334 (1968).
[46] Y. Nakanishi, T. Sakon, M. Motokawa, M. Ozawa, and T. Suzuki, Phys. Rev. B **69**, 024412 (2004).
[47] F. Tang, X. Shen, J. Zhou, S. Cong, L. Zhang, W. Zhou, Z.-D. Han, B. Qian, X.-F. Jiang, R.-K. Zheng, W. Zhao, X.-C. Kan, J. Tang, Y.-Y. Han, X.-Q. Ying, Y. Fang, and S. Ju, Mater. Today Phys. **24**, 100657 (2022).
[48] K. Takegahara, H. Takahashi, A. Yanasa, and T. Kasuya, Solid State Commun. **39**, 857 (1981).
[49] K. Takegahara, H. Takahashi, A. Yanase, and T. Kasuya, J. Phys. C: Solid State Phys. **14**, 737 (1981).
[50] B. Tomasello, C. Castelnovo, R. Moessner, and J. Quintanilla, Phys. Rev. B **92**, 155120 (2015).
[51] N. H. Andersen, J. K. Kjems, and O. Vogt, J. Phys. C: Solid State Phys. **13**, 5137 (1980).
[52] G. Busch and O. Vogt, Phys. Lett. **22**, 388 (1966).
[53] See Supplemental Material at http://link.aps.org/supplemental/10.1103/PhysRevB.106.115137 for HoSb's single-crystal XRD pattern, EDX spectrum, SEM image, elemental distributions, angular M and MR at different T, MR isotherms up to 9 T at different φs and 2 K, M isotherms at different φs and 2 K, angular M under 7 T and its fit with $M = M_s \cos\varphi$ at the FM state around the primary axes and with $M = M_s\sqrt{\frac{1}{2}}\sin(\varphi + \frac{\pi}{4})$ at the HoP-type AFM state around $(2n+1)\pi/4$ ($n = 0, 1, 2$, and 3), and band structures and FS for the FM and HoP-type AFM states, which includes Ref. [54].
[54] P. M. C. Rourke and S. R. Julian, Comput. Phys. Commun. **183**, 324 (2012).
[55] L. S. Silva, S. G. Mercena, D. J. Garcia, E. M. Bittar, C. B. R. Jesus, P. G. Pagliuso, R. Lora-Serrano, C. T. Meneses, and J. G. S. Duque, Phys. Rev. B **95**, 134434 (2017).
[56] G. E. Everett and P. Streit, J. Magn. Magn. Mater. **12**, 277 (1979).
[57] T. O. Brun, F. W. Korty, and J. S. Kouvel, J. Magn. Magn. Mater. **15**, 298 (1980).
[58] N. Kumar, C. Shekhar, J. Klotz, J. Wosnitza, and C. Felser, Phys. Rev. B **96**, 161103(R) (2017).
[59] J.-M. Zhang, F. Tang, Y.-R. Ruan, Y. Chen, R.-W. Zhang, W.-T. Guo, S.-Y. Chen, J.-P. Li, W. Zhao, W. Zhou, L. Zhang, Z.-D. Han, B. Qian, X.-F. Jiang, Z.-G. Huang, D. Qian, and Y. Fang, J. Mater. Chem. C **9**, 6996 (2021).
[60] B. Schrunk, Y. Kushnirenko, B. Kuthanazhi, J. Ahn, L.-L. Wang, E. O'Leary, K. Lee, A. Eaton, A. Fedorov, R. Lou, V. Voroshnin, O J. Clark, J. Sánchez-Barriga, S. L. Bud'ko, R.-J. Slager, P. C. Canfield, and A. Kaminski, Nature (London) **603**, 610 (2022).
[61] Y. Arai, K. Kuroda, T. Nomoto, Z. H. Tin, S. Sakuragi, C. Bareille, S. Akebi, K. Kurokawa, Y. Kinoshita, W.-L. Zhang, S. Shin, M. Tokunaga, H. Kitazawa, Y. Haga, H. S. Suzuki, S. Miyasaka, S. Tajima, K. Iwasa, R. Arita, and T. Kondo, Nat. Mater. **21**, 410 (2022).
[62] R. B. van Dover, E. M. Gyorgy, R. J. Cava, J. J. Krajewsky, R. J. Felder, and W. F. Peck, Phys. Rev. B **47**, 6134 (1993).
[63] Y. Xiao, Y. Su, S. Nandi, S. Price, B. Schmitz, C. M. N. Kumar, R. Mittal, T. Chatterji, N. Kumar, S. K. Dhar, A. Thamizhavel, and Th. Brückel, Phys. Rev. B **85**, 094504 (2012).
[64] A. K. Rajarajan, S. B. Roy, and P. Chaddah, Phys. Rev. B **56**, 7808 (1997).
[65] M. D. Wilding and E. W. Lee, Proc. Phys. Soc. **85**, 955 (1965).
[66] M. Ozawa, T. Matsumura, A. Uesawa, T. Suzuki, T. Sakon, Y. Nakanishi, H. Nojiri, and M. Motokawa, Physica B (Amsterdam) **230**, 744 (1997).